Journal of Engineering and Applied Research (JEAR)

National University of Skills

Summer & Autumn 2025, Vol. 2, No. 2, p. 49- 63

Journal Homepage: https://jear.tvu.ac.ir

:10.48301/JEAR.2024.474745.1089

Optical band gap engineering and comparison of conductivity of Nb and Ta-doped Zinc oxide thin films and their application in opto-electronic

Ahmad Kamalianfar

Department of Physics Education, Farhangian University, P.O. Box 14665-889, Tehran, Iran

ARTICLE INFO

Article Type:
Original Research

Received: 02.19.2025
Revised: 04.21.2025
Accepted: 07.08.2025

Keyword:
Transparent conducting oxides
Niobium doping
Tantalum doping
Band gap

***Corresponding Author:**
Ahmad Kamalianfar
Email: a.kamalianfar@cfu.ac.ir

ABSTRACT

A band gap energy, a fundamental concept in electronic devices, governs both their electrical and optical behaviors. The structural, optical, and band structure properties of niobium and tantalum doped ZnO films deposited on glass substrates were studied for their potential application in the opto-electronic. The films were prepared using the pulse laser deposition technique and characterized by various spectroscopic and microanalytical tools. The samples were annealed at 400 °C in a controlled oxygen environment to improve crystalline quality. The X-ray diffraction analysis of doped ZnO thin films confirmed the incorporation of dopants into the ZnO lattice without altering its wurtzite structure. The crystallite size of ZnO, TaZ, and NbZ films was calculated from the Williamson-Hall method to be 86, 60, and 28 nm, respectivily . The optical bandgap energy was also computed as a function of photon energy using the Tauc formula, revealing a direct band gap of approximately 2.28, 2.38, and 2.40 eV for ZnO, TaZ, and NbZ films, respectivily . A small blue shift in the optical band gap, called the Burstein-Moss shift, was observed in the absorption spectrum, which is often expected in semiconductors with doping. The temperature dependence of the resistivity of the thin films was also investigated. The results showed that the electrical resistances of the films decrease with an increase in temperature.

E-ISSN: 3060-6357

Introduction

Transparent conducting oxides (TCOs) thin films are the fundamental components that exhibit simultaneously high visible wavelength transparency and electrical conductivity. They are widely used in semiconductor lasers, low emissivity windows, photovoltaic cells, and light emitting diodes [1-3]. Semiconducting metal oxides exhibit several attractive features such as high sensitive electrical resistance, low cost, high dielectric constants, excellent chemical and thermal stability, and the ability to tune the energy band gaps of materials [4-6].

Among all oxide materials, zinc oxide (ZnO), being an affordable semiconducting metal oxide is a unique and important semiconductor due to its valuable and huge applications in the areas of sensors, optoelectronics, and energy storage applications [7-9]. However, the limitations of the low electrical properties of ZnO become more critical with the further applications, requiring the improvement of its electrical conductivity without affecting its high transparency.

Band-gap engineering is an effective approach, by which impurities can introduce energy levels within the band gap of the material for the design of new semiconductor materials and devices [10-13]. To the best of our knowledge, there are few reports about doping vanadium group elements, including vanadium (V), niobium (Nb), tantalum (Ta) and dubnium (Db). For example, Jingzhen Shao et al. [14] synthesized Nb-doped ZnO thin films via PLD method. They showed that the produced films with 0.46 at.% Nb content had the lowest resistivity of $8.95 \times 10{-}4\ \Omega$. cm and high transmittance of about 80% with high c-axis orientation. J.M.P. Silva al. [15] reported that after doping of Nb in ZnO, an increase in antimicrobial effect and photocatalytic at about 93.8% (MB) and 88% (CV) was observed. L. Derbali [16] deposited transparent conducting V-doped zinc oxide thin films on FTO substrates using the spray pyrolysis technique and indicated that with increasing V amounts, the band gap was decreased from 3.26 eV to 3.17 eV for 4 at.% of V content. Xu Huang et al. [17] sputtered Ta doped ZnO film on a measuring electrode to form gas sensor and observed that the sample not only enhanced the response but also decreased the response/recovery time and improved the selectivity.

In the recent years, many techniques have been used to synthesize tin oxide films, such as thermal evaporation [18], magnetron sputtering [19], and chemical vapor deposition [20]. Among various thin film fabrication methods, the pulsed laser deposition (PLD) technique is a powerful tool for fabricating ZnO films at the atomic scale.

In previous work [21] we showed that among other thin film deposition techniques, PLD is a powerful tool for fabricating ZnO films that utilizes a pulsed laser beam to ablate a target material, creating a plasma plume that deposits the material onto a substrate. It has superior advantages including a controllable rate of film deposition by adjusting the laser parameters, deposition time, target to substrate distance, deposition time.

In this article, we report the effect of Nb and Ta elements on the structural and optical, and electrical properties of ZnO thin films deposited on glass substrates by pulsed laser deposition (PLD). We focus on the band gap of the obtained films, as a fundamental quantity that directly relates to the usability of materials in optical, electronic, and energy applications.

Band Theory of Semiconductors

Knowledge of the electronic band structure of a semiconductor provides information about its electrical and optical properties and often estimates which transitions occur under illumination. Semiconductors include two main charge carriers, free electrons and positive holes. Semiconductor materials are classified as N-type and P-type (see Figure 1a). N-type semiconductors mainly use electrons as charge carriers, while p-type semiconductors have an excess of holes where an electron could exist. In solid-state physics, electrons of the same energy states form bands. The valence band is the highest range of electron energies with energy Ev, which can be occupied by an electron, and the lowest unoccupied band is the conduction band with energy Ec. The energy difference between the top of the valence band and the bottom of the conduction band is called the band gap.

To describe the relationship between optical absorbance and band gap energy, optical band gap can be estimated using the following Tauc relation [22]:

$$(\alpha h\upsilon)^{1/n} = A(h\upsilon - E_g)$$

where h is Plank's constant, υ is photon frequency, Eg is band gap energy, A is a constant, n is a factor that depends on the nature of the electronic transition between the valance band and conduction band, and α is the absorbance coefficient. The factor n may have values of n = ½ for direct (allowed) transitions, n = 3/2 for direct (forbidden) transitions, n = 2 for indirect (allowed) transition, n = 3 for indirect (forbidden) transitions [23].

In a direct band gap semiconductor, the minimum of the conduction band coincides with the maximum of the valence band and the carrier transitions between them occur without change in momentum of the two states involved. In

opposite, for an indirect bandgap semiconductor the minimum conduction band energy and maximum valence band energy occur at different crystal momentums [24]. Figure 1b illustrates

In conductors, there are no band gaps between the valence and conduction bands, due to the overlap in the bands. Insulators have a large band gap (up to 7eV) between the valence and conduction bands. The difference between these two bands for semiconductors is less than 3 eV.

An intrinsic semiconductor is a pure material with a small band gap and its Fermi level is in the middle of the band gap, while extrinsic semiconductors have larger band gaps, and the band gap is controlled by purposefully adding (doping) small impurities to the material.

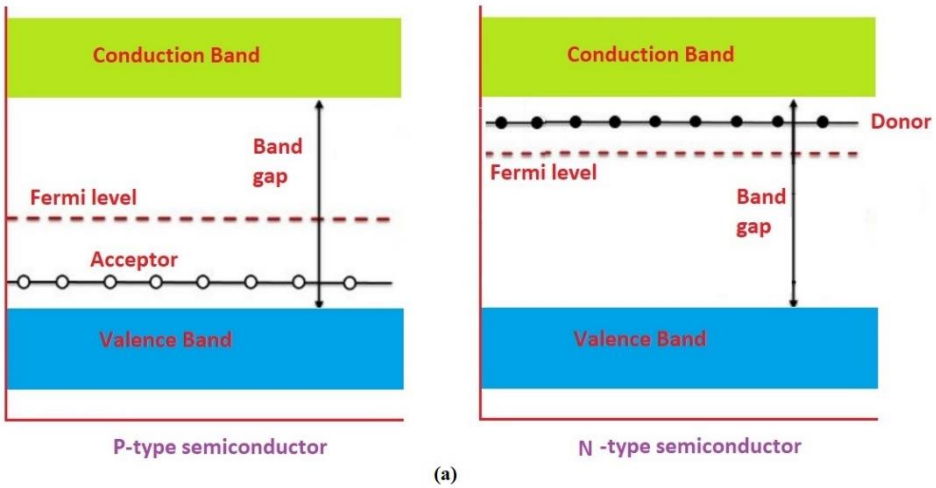

(a)

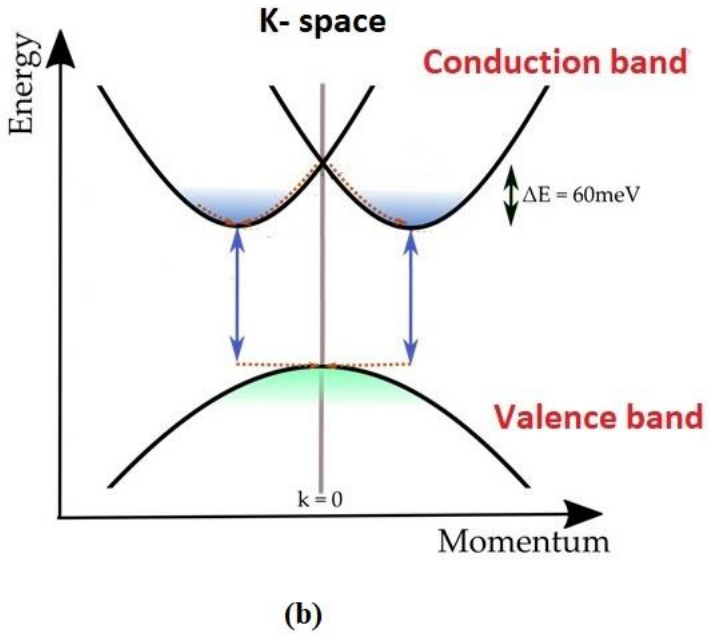

Figure 1. (a) Comparison of P-type and n-type semiconductors, (b) Direct and Indirect band gaps.

Experimental method

The targets of NaZ and TaZ were prepared by a solid-state reaction method using ZnO mixed with Nb2O5 and Ta2O5 powers in stoichiometric mass ratios, which was 1:49 for 2 wt% doping. The mixed powders were combined and ground for 5 hours. Homogeneous powders were shaped and pressed with a hydraulic press into pellets (diameter 20 mm and thickness about 5 mm) and sintered at 900 °C for 5 hour in a heating furnace. The cleaned glass substrates were held on a sample holder and placed in the chamber. The ablation process was performed employing a Nd-YAG pulsed laser with a beam wavelength of 532 nm, a pulse width of 6 ns, fluence ~7 J/cm2, and a 10 Hz repetition rate. To reduce oxide formation in the deposited films, the chamber was evacuated to a residual pressure lower than10^{-4}Pa. The deposition time was 10 minutes, and the distance between the target surface and the glass substrate was 5 cm. To improve the crystallinity of the thin films, we have done post deposition annealing for 20 min in a vacuum. A schematic diagram of the PLD system is shown in Figure 2.

Finally, we performed a vacuum annealing at 400 °C, in order to improve the crystallinity of thin film samples with identities ZnO, Nb doped ZnO (NbZ), and Ta doped ZnO (TaZ).

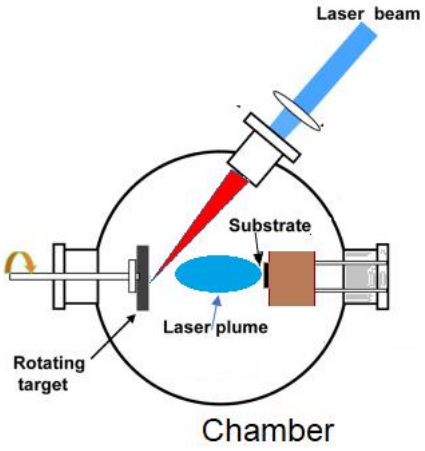

Figure 2. The schematic diagram of the PLD.

The crystalline structure of the undoped and doped ZnO films was characterized by X-ray Diffraction (XRD, PANalytical Philips X'pert Pro, λ = 0.154 nm).) using the 2θ–θ scan with CuKα radiation. The surface morphologies of films were observed using scanning electron microscopy (SEM, Jeol 6500). An ultraviolet/visible/near-infrared (UV/VIS/NIR) spectrophotometer (JASCO) was used to measure the optical bandgap of the films. The resistance measurement was performed using the standard four-probe method from 60 to 300 K.

Result and discussion

The structural study of the films was examined using XRD and is represented in Figure 3. All samples show high crystallinity due to their clear and sharp peaks. The diffraction peaks of (100), (002), (101), (102), and (110) appeared and matched with the International Centre for Diffraction Data reference code (01-076-0704). There were no traces of any secondary phase, niobium, or tantalum in the samples for a doping concentration of 2 w%, indicating that the diffraction peaks are corresponding to the wurtzite-structure.

The average crystallite size of the samples was calculated using the well-known Scherrer equation [25]:

$$D = \frac{k\lambda}{\beta_{hkl}\cos\theta} \qquad (1)$$

$$\frac{cos\theta}{\lambda} = \frac{k}{D\beta_{hkl}} \qquad (2)$$

where β_{hkl} is the full-width half maximum, k (=0.94) is the Scherrer constant, D is the crystallite size, the peak position (θ), and λ (=1.54 A^o) is the wavelength of X-ray.

In addition, according to Williamson-Hall Method, β_{hkl} depends on the both size of the crystallites and the strain of the lattice [26].

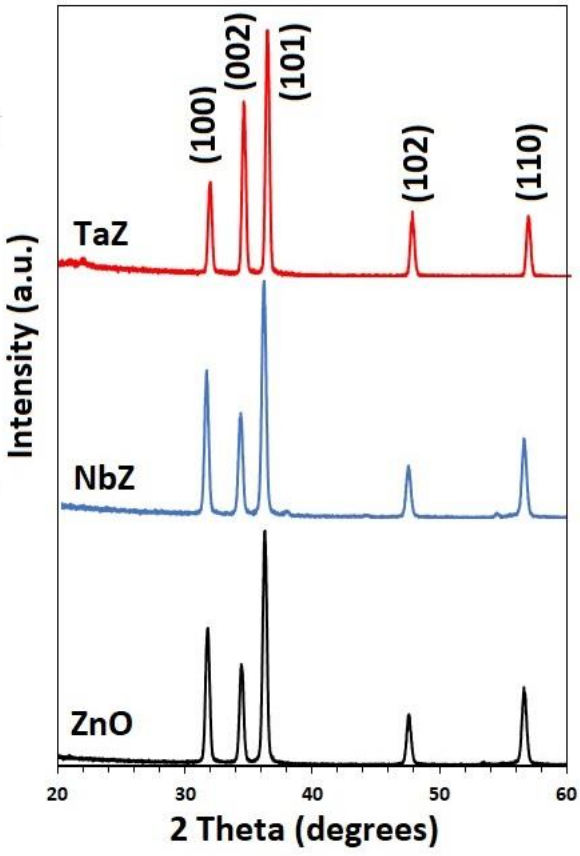

Figure 3. XRD patterns of of pure and doped ZnO thin films.

The crystal imperfections and distortion of strain-induced peak broadening can be obtained from $\epsilon = \frac{\beta_{hkl}}{tan\theta}$, and the following result, which is the addition of the Scherrer equation and the strain [27]:

$$\beta_{hkl} = \frac{k\lambda}{D} + 4\epsilon\, sin\theta \quad (3)$$

Thus, the crystallite size and strain are determined from the slope and y-intercept of the plot of $\frac{cos\theta}{\lambda}$ against $\frac{1}{\beta_{hkl}}$.

Table 1. Crystallite size (D) and band gap of pure and doped ZnO thin films.

Sample	(hkl)	2θ (degree)	FWHM (degree)	Crystallite size (nm)±1 Schere	Crystallite size (nm)±1 W-H	Band gap (eV)
ZnO	(100)	31.6412	0.0960	95	86	3.28
	(002)	34.3333	0.1108	81		
	(101)	36.2170	0.1148	87		
	(102	47.5154	0.0990	91		
TaZ	(100)	31.7984	0.1574	59	60	3.38
	(002)	34.4047	0.1574	61		
	(101)	36.2773	0.3149	31		
	(102)	47.6449	0.1181	99		
NbZ	(100)	31.6412	0.1118	83	28	3.40
	(002)	34.3333	0.1233	78		
	(101)	36.2170	0.1312	75		
	(102)	47.5154	0.1305	90		

These results indicate that the incorporation of impurity ions into the film structure results in shift of the characteristic diffraction peaks to lower or higher 2θ angles, broadening of the FWHM, and variation in the diffraction intensities. For example, the average crystallite size decreases in the TaZ and NbZ thin films compared to the pure one. Additionally, the XRD patterns show that Ta doping resulted in an increase in the intensity of the (002) peak relative to that of the undoped ZnO nanostructure. The decrease in crystallite size is due to the doping of Ta and Nb into the ZnO lattice, which prevents crystallite growth, possibly slows down the formation of grain boundaries, and/or modifies the rate of nucleation during the sample crystallization.

The morphologies of the ZnO, NbZ and TaZ are explored through the scanning electron microscope (Figure 4. a–c). The surface of the films shows a porous structure morphology. Some of particles are agglomerated into nearly spherical

and platelet structures. Previous research has shown that the multiple-shaped porous structure, and larger surface-to-volume ratios have the potential to enhance the functionality of ZnO for applications in light-emitting [28,29].

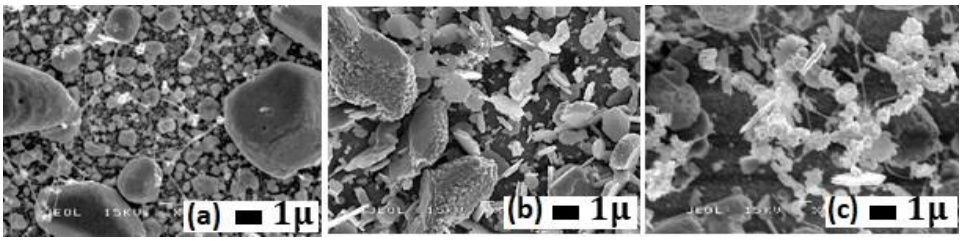

Figure 4. SEM image of of (a) ZnO, (b) NbZ, (c) TaZ thin films.

Figure 5. shows the EDX spectra of Nb and Ta doped ZnO thin films. The strong peaks of Zn and O were detected in the EDX spectra, confirming the formation of ZnO as the final product with Nb and Ta as impurities.

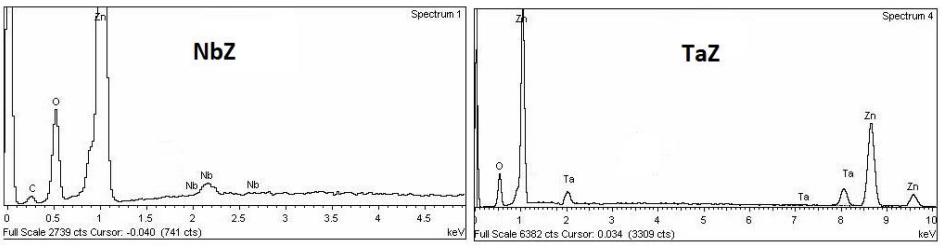

Figure 5. The EDX spectra of Nb and Ta doped ZnO thin films.

Optical study

UV/Vis absorption of the samples, deposited on a glass substrate was provided as a function of wavelength (nm) in the spectral range 300 nm to 700 nm as shown in Figure 6. Absorption in the UV region is attributed to band gap absorption of the thin films. The doped ZnO films exhibited an absorption band edge that was more similar to the absorption of ZnO. There is not much difference in absorbance values because as mentioned in the literature, Nb and Ta elements have very similar properties. However, the absorption edge was found to be blue-shifted for doped ZnO thin films.

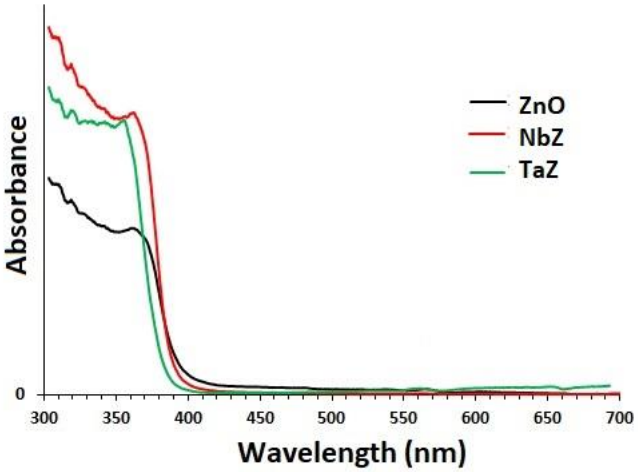

Figure 6. variation of (αhv)2 versus hv of pure and doped ZnO thin films.

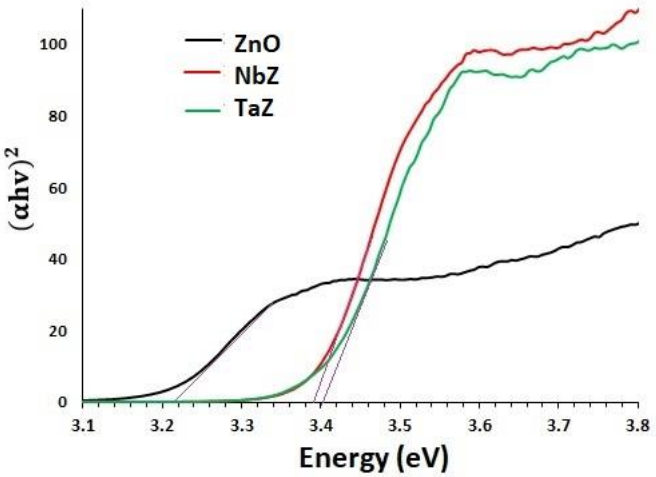

Figure 7. UV–Vis absorption spectra of pure and doped ZnO thin films.

The optical band gap, Eg, can be calculated using absorption edge values. According to Tauc's relation, the direct bandgap value can be extrapolated by fitting a straight line to the plot of (αhυ)^ (1/2) versus the photon energy (hυ), as shown in Figure 7. The optical bandgap energies for the ZnO, TaZ, and NbZ films are equal to 3.32, 3.38, and 3.40 eV, respectively.

The band gap of a material is influenced by various factors, including crystallite size, carrier concentration, and the presence of strain. The expansion of band gap values can be attributed to the filling of the lowest states in the conduction band, a phenomenon well explained by the Burstein-Moss effect [30]. In optical studies of doped materials, this effect manifests as an upward shift in the absorption edge (a blue shift of the band gap towards higher energies) following doping [31]. Such a shift in the optical band gap underscores the potential of band gap manipulation in ZnO through doping with elements like Ta and Nb. Band gap engineering is crucial for fine-tuning energy levels in optoelectronic devices [32]. The primary mechanism for this adjustment involves controlling the doping process, which modifies electron transfer properties through alterations in the crystalline structure of metal oxides. These modifications may result from changes in lattice parameters or from dopants serving as electron traps that hinder charge recombination, or possibly through the introduction of an intermediate energy level between the conduction and valence bands. Often, shifts in the conduction band edge induced by doping arise from disturbances to the lattice structure of the base metal oxides caused by the dopants. Nonetheless, the degree of these changes is contingent upon the level and distribution of doping.

Electrical study

The temperature dependence of resistivity was measured using the four-probe method in the temperature range from 60 to 300 K. As shown in Figure 8, the normalized electrical resistances of the films decrease with increasing in temperature. The decrease in resistivity was faster for NaZ and TaZ films compared to the undoped ZnO film. The films exhibit basically a semiconductor-type conduction behavior as expected, due to the increased occupancy of charge carriers in the conduction band of semiconductors.

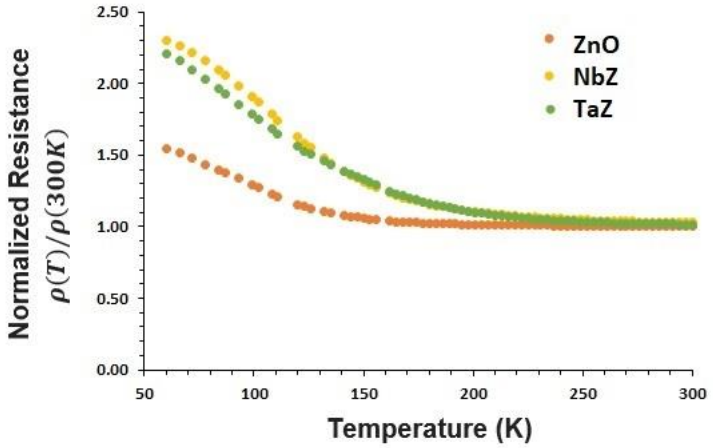

Figure 8. Temperature dependence of the normalized electrical resistances of pure and doped ZnO thin films.

A wide optical bandgap (Eg>3.2 eV) and an increase in electrical conductivity indicate that when the films are used in an optoelectronic device their absorption losses can be minimized.

Conclusion

This present research work comprised of structural, morphological, electrical and optical analysis of pure ZnO, 2 % Nb-doped, and Ta-doped ZnO thin films obtained using the PLD method on a glass substrate.

The XRD patterns revealed that Nb and Ta doping did not change the crystal structure of ZnO thin films, but the crystallite size of the ZnO film decreased with Ta and Nb doping. The normalized electrical resistances of the doped films decreased from 2.4 to about 1 with the increases in temperature. The band gap of the ZnO films increasing from 2.28 to 3.38 and 3.40 for Ta-doped ZnO and Nb doped ZnO films, respectivily . This band gap engineering, following a decrease in resistivity, may find potential applications in the fabrication of various devices based on optoelectronics.

Disclosure statement and funding

The authors declare no potential conflicts of interest. The present study received no financial support from any organization or institution.

References

[1] Koida, T., & Nomoto, J. (2024). Sustainable Transparent Conducting Oxides: Insights from Amorphous SnOx Thin Films via Oxygen Stoichiometry Control. *Chemistry of Materials*, *36*(14), 6838-6848. https://doi.org/10.1021/acs.chemmater.4c00719

[2] Chavan, G. T., Kim, Y., Khokhar, M. Q., Hussain, S. Q., Cho, E.-C., Yi, J., Ahmad, Z., Rosaiah, P., & Jeon, C.-W. (2023). A Brief Review of Transparent Conducting Oxides (TCO): The Influence of Different Deposition Techniques on the Efficiency of Solar Cells. Nanomaterials, 13(7), 1226. https://www.mdpi.com/2079-4991/13/7/1226

[3] Balaprakash, V., Thangavel, K., Mohan, M., Gowrisankar, P., & Sakthivel, R. (2024). Thin Film Transparent Conducting Oxides and its Anticorrosion and Surface Protection Applications. In Novel Anti-Corrosion and Anti-Fouling Coatings and Thin Films (109-127). https://doi.org/https://doi.org/10.1002/9781394234318.ch5

[4] Gao, L., Tian, Y., Hussain, A., Guan, Y., & Xu, G. (2024). Recent developments and challenges in resistance-based hydrogen gas sensors based on metal oxide semiconductors. Analytical and Bioanalytical Chemistry, 416(16), 3697-3715. https://doi.org/10.1007/s00216-024-05213-z

[5] Amdouni, S., Aouassa, M., Bouaabdellaoui, M., Aladim, A. K., & Yahyaoui, M. (2024). Electrical and dielectric properties of ferromagnetic GeMn nanocrystals embedded in metal-oxide-semiconductor Schottky diodes (Al/SiO2:GeMn NCs/n-Si) grown by MBE. Vacuum, 224, 113191. https://doi.org/https://doi.org/10.1016/j.vacuum.2024.113191

[6] Jawad, M., Ur Rahman, A., Hussain Mirza, S., Azam, S., Khalifa, M. E., & El-Bahy, S. M. (2024). From wide band gap semiconductor to visible light responsive material: The role of Li in K2PdO2. Chemical Physics, 585, 112367. https://doi.org/https://doi.org/10.1016/j.chemphys.2024.112367

[7] Kamalianfar, A. (2023). Promotional effects of Ag decoration on root-like ZnO microstructures for ethanol sensing. Journal of Materials Science: Materials in Electronics, 34(17), 1338. https://doi.org/10.1007/s10854-023-10678-2

[8] Saadi, H., Benzarti, Z., Sanguino, P., Pina, J., Abdelmoula, N., & de Melo, J. S. S. (2023). Enhancing the electrical conductivity and the dielectric features of ZnO nanoparticles through Co doping effect for energy storage applications. Journal of Materials Science: Materials in Electronics, 34(2), 116. https://doi.org/10.1007/s10854-022-09470-5

[9] Zhang, T., Li, M., Chen, J., Wang, Y., Miao, L., Lu, Y., & He, Y. (2022). Multi-component ZnO alloys: Bandgap engineering, hetero-structures, and optoelectronic devices. *Materials Science and Engineering: R: Reports*, *147*, 100661. https://doi.org/https://doi.org/10.1016/j.mser.2021.100661

[10] Fernandes, J., Kalluri, S., Alsuwaidi, M., Mayakrishnan, V., Mohan, C., & Madhavan, A. A. (2024). Band gap engineering of g-C3N4/CuS and its application in Solar Still. *Chemical Physics Impact*, *9*, 100684. https://doi.org/https://doi.org/10.1016/j.chphi.2024.100684

[11] Su, D., Cheng, J., Li, S., Zhang, S., Lyu, T., Zhang, C., Li, J., Liu, F., & Hu, L. (2023). Inhibiting the bipolar effect via band gap engineering to improve the thermoelectric performance in n-type Bi2-xSbxTe3 for solid-state refrigeration. *Journal of Materials Science & Technology*, *138*, 50-58. https://doi.org/https://doi.org/10.1016/j.jmst.2022.07.048

[12] Pozzi, M., Jonak Dutta, S., Kuntze, M., Bading, J., Rüßbült, J. S., Fabig, C., Langfeldt, M., Schulz, F., Horcajada, P., & Parak, W. J. (2024). Visualization of the High Surface-to-Volume Ratio of Nanomaterials and Its Consequences. Journal of Chemical Education, 101(8), 3146-3155. https://doi.org/10.1021/acs.jchemed.4c00089

[13] Oh, Y., Song, S., & Bae, J. (2024). A Review of Bandgap Engineering and Prediction in 2D Material Heterostructures: A DFT Perspective. International Journal of Molecular Sciences, 25(23), 13104. https://www.mdpi.com/1422-0067/25/23/13104

[14] Sun, H., Kim, H., Xu, X., Fei, L., Jung, W., & Shao, Z. (2023). Thin Films Fabricated by Pulsed Laser Deposition for Electrocatalysis. *Renewables*, *1*(1), 21-38. https://doi.org/doi:10.31635/renewables.022.202200002

[15] Silva, J. M. P., Julião, R. S., Nicácio, T. C. N., Melo, M. C. N., Santos, R. M., Bomio, M. R. D., & Motta, F. V. (2024). A study of Nb-doped ZnO ceramic and its enhanced solar photocatalysis, photoluminescence and antimicrobial properties. Journal of Alloys and Compounds, 985, 173978. https://doi.org/https://doi.org/10.1016/j.jallcom.2024.173978

[16] Derbali, L., Bouhjar, F., & Derbali, A. (2024). Photocurrent performance and enhancement of opto-electronic properties of spray pyrolysis deposited ZnO thin films via V-doping. *Modern Physics Letters B*, *38*(09), 2450060. https://doi.org/10.1142/s021798492450060x

[17] Huang, X., Li, C., Qian, L., Li, M., Li, H., Niu, X., & Yang, B. (2019). Improved ethanol vapor sensing properties of sputtered ZnO films by doping Ta. Materials Today Communications, 21, 100680. https://doi.org/https://doi.org/10.1016/j.mtcomm.2019.100680

[18] Dastan, D., shan, K., Jafari, A., Marszalek, T., Mohammed, M. K. A., Tao, L., Shi, Z., Chen, Y., Yin, X.-T., Alharbi, N. D., Gity, F., Asgary, S., Hatamvand, M., & Ansari, L. (2023). Influence of heat treatment on H2S gas sensing features of NiO thin films deposited via thermal evaporation technique. *Materials Science in Semiconductor Processing*, *154*, 107232. https://doi.org/https://doi.org/10.1016/j.mssp.2022.107232

[19] Zhou, J., Zhang, S., & Wang, J. (2024). Magnetron sputtered transition-metal-nitrides thin films as electrode materials for supercapacitors: A review. *Journal of Energy Storage*, *104*, 114476. https://doi.org/https://doi.org/10.1016/j.est.2024.114476

[20] Kamalianfar, A., Naseri, M. G., & Jahromi, S. P. (2019). Preparation and gas-sensing performances of Cr2O3-decorated ZnO nanostructures grown in a boundary layer of non-uniform thickness for low-working temperature H2S detection. Chemical Physics Letters, 732, 136648. https://doi.org/https://doi.org/10.1016/j.cplett.2019.136648

[21] Kamalianfar, A. (2024). Study of Pristine and Ni-Doped ZnO Nanorods Synthesized by Pulse Laser Deposition. *Quarterly Journal of Optoelectronic*, *7*(2), 49-54. https://doi.org/10.30473/jphys.2024.72650.1218

[22] Makuła, P., Pacia, M., & Macyk, W. (2018). How To Correctly Determine the Band Gap Energy of Modified Semiconductor Photocatalysts Based on UV−Vis Spectra. The Journal of Physical Chemistry Letters, 9(23), 6814-6817. https://doi.org/10.1021/acs.jpclett.8b02892

[23] Haryński, Ł., Olejnik, A., Grochowska, K., & Siuzdak, K. (2022). A facile method for Tauc exponent and corresponding electronic transitions determination in

semiconductors directly from UV–Vis spectroscopy data. *Optical Materials*, *127*, 112205. https://doi.org/https://doi.org/10.1016/j.optmat.2022.112205

[24] Sharaf, O. Z., & Orhan, M. F. (2015). Concentrated photovoltaic thermal (CPVT) solar collector systems: Part I – Fundamentals, design considerations and current technologies. *Renewable and Sustainable Energy Reviews*, *50*, 1500-1565. https://doi.org/https://doi.org/10.1016/j.rser.2015.05.036

[25] Alam, M. K., Hossain, M. S., Bahadur, N. M., & Ahmed, S. (2024). A comparative study in estimating of crystallite sizes of synthesized and natural hydroxyapatites using Scherrer Method, Williamson-Hall model, Size-Strain Plot and Halder-Wagner Method. *Journal of Molecular Structure*, *1306*, 137820. https://doi.org/https://doi.org/10.1016/j.molstruc.2024.137820

[26] Disha, S. A., Sahadat Hossain, M., Habib, M. L., & Ahmed, S. (2024). Calculation of crystallite sizes of pure and metals doped hydroxyapatite engaging Scherrer method, Halder-Wagner method, Williamson-Hall model, and size-strain plot. *Results in Materials*, *21*, 100496. https://doi.org/https://doi.org/10.1016/j.rinma.2023.100496

[27] Nadjia, L., & Abdelkader, E. (2025). Design, synthesis and characterization of ceria: assessment of crystallite size and intrinsic strain using XRD profile analysis and its photocatalytic applications. *Journal of the Iranian Chemical Society*, *22*(2), 297-324. https://doi.org/10.1007/s13738-024-03149-w

[28] Purbayanto, M. A. K., Rusydi, A., & Darma, Y. (2020). The effect of crystallinity on the surface modification and optical properties of ZnO thin films [10.1039/C9CP05464B]. *Physical Chemistry Chemical Physics*, *22*(4), 2010-2018. https://doi.org/10.1039/C9CP05464B

[29] Raha, S., & Ahmaruzzaman, M. (2022). ZnO nanostructured materials and their potential applications: progress, challenges and perspectives [10.1039/D1NA00880C]. *Nanoscale Advances*, *4*(8), 1868-1925. https://doi.org/10.1039/D1NA00880C

[30] ullah, R., Khan, M. T., Iqbal, A. M., & Li, X. (2024). Exploring the synergistic influence of Cu and Co co-doping on the optical properties of ZnO nanoparticles. *Optical Materials*, *147*, 114719. https://doi.org/https://doi.org/10.1016/j.optmat.2023.114719

[31] Zhou, X., Huang, E., Zhang, R., Xiang, H., Zhong, W., & Xu, B. (2023). Multicolor Tunable Electrochromic Materials Based on the Burstein–Moss Effect. *Nanomaterials*, *13*(10), 1580. https://www.mdpi.com/2079-4991/13/10/1580

[32] Kumawat, A., Chattopadhyay, S., Misra, K. P., Halder, N., Jain, S. K., & Choudhary, B. L. (2020). Blue-shift in the optical band gap of sol-gel derived Zn(1-x)SrxO nanoparticles. *Solid State Sciences*, *108*, 106379. https://doi.org/https://doi.org/10.1016/j.solidstatesciences.2020.106379